

# Superhard Properties of Rhodium and Iridium Boride Films

Alessandro Latini,<sup>†</sup> Julietta V. Rau,<sup>\*,†</sup> Roberto Teghil,<sup>§</sup> Amanda Generosi,<sup>‡</sup> and Valerio Rossi Albertini<sup>†</sup>

Dipartimento di Chimica, "Sapienza" Università di Roma, Piazzale Aldo Moro, 5, 00185 Rome, Italy, Istituto di Struttura della Materia, Consiglio Nazionale delle Ricerche, Via del Fosso del Cavaliere, 100, 00133 Rome, Italy, and Dipartimento di Chimica, Università della Basilicata, via N. Sauro 85, 85100, Potenza, Italy

**ABSTRACT** Very recently, the superhard properties of rhenium and ruthenium boride films were reported, this research being inspired by the discovery of the  $\text{ReB}_2$  bulk superhardness. In this paper, we report the first successful deposition and characterization of rhodium and iridium boride films, other possible candidates for superhard materials. The films were prepared, applying the pulsed laser deposition technique, and studied by X-ray diffraction, scanning electron and atomic force microscopies, and Vickers microhardness. The refined structural parameters for  $\text{RhB}_{1,1}$  and  $\text{IrB}_{1,1}$  films were obtained. The  $\text{RhB}_{1,1}$  film is characterized by the submicrometer crystallite size, whereas for the  $\text{IrB}_{1,1}$  film, the crystallite size is in the tens of nanometers range, and this latter film presents a slightly preferred orientation along the [004] direction. Both the films exhibit very similar morphology, being composed of dense globular aggregate texture. The  $\text{RhB}_{1,1}$  film presents a homogeneously textured surface with an average roughness of 20–50 nm, whereas the  $\text{IrB}_{1,1}$  film possesses a finer texture with an average roughness of 20–30 nm. The intrinsic hardness of both films lies in the superhardness range: the 1.0  $\mu\text{m}$  thick  $\text{RhB}_{1,1}$  film possesses a hardness of 44 GPa, whereas the 0.4  $\mu\text{m}$  thick  $\text{IrB}_{1,1}$  film has a hardness of 43 GPa.

**KEYWORDS:** rhodium boride film • iridium boride film • hardness • superhard • pulsed laser deposition

## 1. INTRODUCTION

Hardness is a complex material's parameter indicating the resistance to both plastic and elastic deformations. Superhard (hardness  $\geq 40$  GPa (1)) materials and coatings are of great interest for the scientific community from the point of view of both basic research and their numerous industrial applications, ranging from cutting tools to wear-resistant coatings. One of the recently developed groups of superhard materials are compounds of transition metals with light elements, such as B, C, N, and O. Many of the compounds belonging to this group, such as most carbides and borides, can be synthesized in a quite simple way, via arc or electron beam melting under vacuum or at ambient pressure. Very recently, several compounds belonging to this group and their hard and superhard properties were discussed (2–8). Two design parameters were outlined to be of the most importance for the selection of compounds, possessing exceptional superhard properties, such as combination of high valence electron density and the presence of short covalent bonds (4, 9).

An attempt to define a trend in the structure-hardness properties of borides of the fifth and sixth period transition metals, has been recently discussed by us in ref 8. It was

hypothesized that the observed trend could be explained taking into account the electronic structure, and namely, the factors influencing the bond strength, like better overlap between outer d orbitals of transition metals and 2p orbitals of boron. The same idea was expressed and developed by authors (10) reporting that the trends in hardness of transition metal diborides are controlled by the relativistic effects that result in better orbital overlap of the transition metal outer d orbitals and the 2p orbitals of boron, and as a consequence, increased bond strength.

Recently, we reported the first successful preparation of thin  $\text{ReB}_2$  and biphasic  $\text{RuB}_2$ – $\text{Ru}_2\text{B}_3$  films applying the pulsed laser deposition (PLD) technique, both possessing superhard properties (11, 12). In this paper, we present the results of the continued research in this field and report the first successful preparation of  $\text{RhB}_{1,1}$  and  $\text{IrB}_{1,1}$  films, carried out applying the same deposition technique used in our earlier works (PLD), and the investigation of their properties by X-ray diffraction (XRD), scanning electron microscopy (SEM) coupled with a system for microanalysis (energy-dispersive X-ray spectroscopy (EDXS)), atomic force microscopy (AFM) and Vickers microhardness measurements.

To the best of our knowledge, up to now there is only one more method described in the literature (13) that has been applied to obtain crystalline coatings of this class of materials. The authors (13) used a tunable IR free electron laser facility for a confined-plume chemical deposition synthesis.

## 2. EXPERIMENTAL SECTION

**2.1. Synthesis of  $\text{RhB}_{1,1}$  and  $\text{IrB}_{1,35}$  Targets.**  $\text{RhB}_{1,1}$  and  $\text{IrB}_{1,35}$  used for the PLD process were synthesized

\* Corresponding author. Tel: +39-06-4993 4086. Fax: +39-06-4993 4153. E-mail: giulietta.rau@ism.cnr.it.

Received for review November 25, 2009 and accepted February 1, 2010

<sup>†</sup> "Sapienza" Università di Roma.

<sup>‡</sup> Consiglio Nazionale delle Ricerche.

<sup>§</sup> Università della Basilicata.

DOI: 10.1021/am9008264

© 2010 American Chemical Society

applying an electron beam synthesis technique, the details of which can be found elsewhere (8, 14). In brief, for  $\text{RhB}_{1.1}$  target preparation, rhodium powder (Engelhard,  $\sim 325$  mesh, purity  $>99\%$ ) and crystalline boron powder (Alfa Aesar,  $\sim 60$  mesh, purity  $99.5\%$ ) in a stoichiometric ratio were carefully mixed in an agate mortar with the addition of some acetone to facilitate intimate mixing. The same procedure was adopted for iridium and boron but, in this case, iridium powder (Chempur,  $<60\ \mu\text{m}$ , purity  $99.9\%$ ) and crystalline boron powder (Alfa Aesar,  $\sim 60$  mesh, purity  $99.5\%$ ) were used in a molar ratio of 1:1.5, respectively, in order to compensate the evaporative loss of boron during the synthesis.

After the mixing and drying procedures, the powders were cold-pressed into pellets (diameter 18 mm). The pellet, contained in a  $\text{TiB}_2/\text{BN}$  composite crucible (GE Advanced Ceramics, UK), was positioned into the pocket of an electron beam gun (model EV1-8, Ferrotec, Germany) inside a high vacuum chamber evacuated by a turbo pump. The pellets were melted two times (the second melting was performed after repositioning of the pellet upside-down), thus ensuring the completeness of the reaction. The pressure inside the chamber during the synthesis was  $\sim 1 \times 10^{-4}$  Pa. For the melting process, an accelerating voltage of the electron beam of  $-3.5$  kV and an emission current in the range of 50–150 mA were used.

**2.2. Pulsed Laser Deposition of Films.** PLD method was applied to deposit rhodium and iridium boride films on a  $\text{SiO}_2$  substrate (1 mm thick optically polished fused silica slides). In this technique, a pulsed laser beam is focused on a target and the sublimated material is collected onto a substrate, placed in a suitable position. Both ablation and deposition were performed by means of an experimental apparatus consisting of a multiport stainless steel vacuum chamber evacuated by a rotary-turbomolecular pumping system down to a pressure of  $4 \times 10^{-4}$  Pa. The chamber is equipped with a support for the target, rotating with a speed of 1 rpm to minimize the “craterization” effects (15), quartz windows for the laser beam inlet, and a resistively heated substrate holder. Targets having the  $\text{RhB}_{1.1}$  and  $\text{IrB}_{1.35}$  composition were used. The  $\text{SiO}_2$  substrate was kept in front of the target at a distance of 2 cm. The ablation laser source was a frequency doubled Nd:glass laser with the following characteristics:  $\lambda = 527$  nm,  $E = 2.35$  mJ, repetition rate = 10 Hz, pulse duration = 250 fs. The laser beam, focused by a suitable optical system, impinged on the target surface with an inclination angle of  $45^\circ$ , the spot area being  $0.1\ \text{mm}^2$ . The film deposition lasted 4 h. The substrates were kept at  $600\ ^\circ\text{C}$  during the deposition, the temperature being measured by a thermocouple attached to the bottom of the substrate holder (error  $\pm 10\ ^\circ\text{C}$ ).

**2.3. X-ray Diffraction.** Rhodium and iridium boride films were analyzed using a Panalytical X'Pert Pro diffractometer (Bragg–Brentano geometry,  $\text{CuK}\alpha$  radiation,  $\lambda = 1.54184\ \text{\AA}$ ) with X-ray tube operating at 1600 W (40 kV, 40 mA), equipped with a gas filled proportional detector.  $\theta$ – $\theta$  scans were performed, using an incident beam slit of  $1^\circ$

angular divergence, coupled with the 10 mm mask for rhodium boride film and the 20 mm mask for iridium boride film, a collimator of 0.04 rad and a Ni filter for the  $\text{K}\beta$  component of the Cu radiation. The diffraction patterns were collected in the angular range of  $20$ – $90^\circ$  for 24 h. Once collected, the diffractograms were analyzed by the MAUD Rietveld software package (16). From the Rietveld analysis, the refined unit-cell parameters, rms microstrain values, and crystallite size were obtained.

**2.4. Scanning Electron Microscopy Measurements.** Scanning Electron Microscopy (a LEO 1450 Variable Pressure) apparatus, working in secondary and backscattered electron modes, was applied for morphological studies of the deposited rhodium and iridium boride films. The SEM apparatus was coupled with a system for microanalysis EDXS INCA 300, allowing to execute qualitative/quantitative analysis of the elements. The film samples for SEM measurements were coated with an ultrathin gold layer. The plane and cross-section view images were obtained, the latter being necessary for the thickness measurements. Because the images of the films thickness were obtained at the sample edge tilted by  $45^\circ$ , the measured values were multiplied by  $\sqrt{2}/2$ . The thickness measurements were carried out in the backscattered electron mode by means of the 4 Quadrants detector. The atomic number contrast, presented in the SEM images as gray color hues, allowed us to precisely distinguish the film boundary and the interface with the  $\text{SiO}_2$  substrate. To confirm the results of the atomic number contrast, we have carried out the EDXS analysis of the chemical nature of the observed phases.

**2.5. Atomic Force Microscopy Measurements.** The AFM measurements were performed in noncontact mode using a noncommercial air-operating atomic force microscope (17). Several portions of the film samples surface were topographically phase-shift reconstructed in order to evaluate the morphological/chemical homogeneity of the deposition, collecting large scale images. Afterward, high-definition topographic zooms were collected from the representative portions of the films, in order to quantitatively study the surface texture and roughness and the aggregate dimensions. To estimate the film thickness, we made a scratch in the film layer and measured its profile in the contact mode.

**2.6. Vickers Microhardness Measurements.** The microhardness measurements were performed by means of a Leica VMHT apparatus (Leica GmbH, Germany), equipped with a standard Vickers pyramidal indenter (square-based diamond pyramid of  $136^\circ$  face angle). The loading and unloading speed was  $5 \times 10^{-6}$  m/s, and the time under the peak load was 15 s. The hardness of the  $\text{SiO}_2$  substrate and the films was measured according to the procedure described in detailed in our previous works (18, 19).

For film samples, the measured hardness was that of the film/substrate composite system. To separate the composite hardness of the film/substrate system ( $H_c$ ) into its components, film ( $H_f$ ) and substrate ( $H_s$ ), we applied a Jönsson and Hogmark model based on area “law-of-mixtures” approach

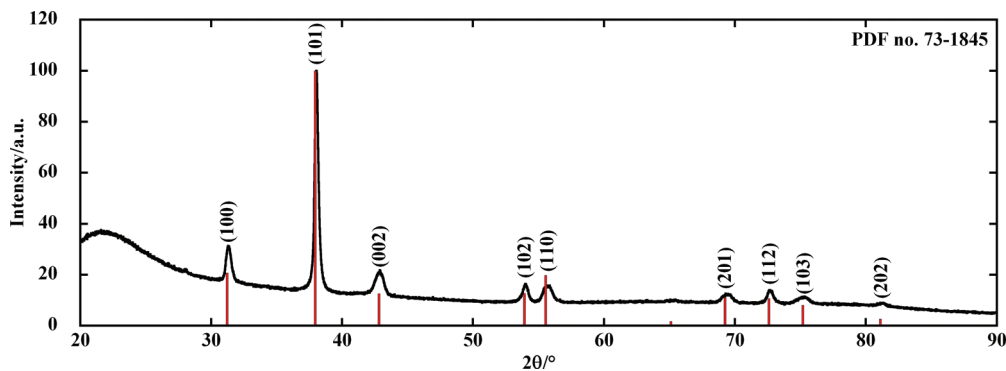


FIGURE 1. X-ray powder diffraction pattern of RhB<sub>1.1</sub> film.

(20), taking into account the indentation size effect (21). In this case, the composite hardness  $H_c$  is expressed as

$$H_c = H_{s0} + [B_s + 2ct(H_{f0} - H_{s0})]/D \quad (1)$$

where  $c \cong 0.5$  for a brittle hard film on a more ductile substrate (20);  $H_{s0}$  and  $H_{f0}$  are the intrinsic hardness of substrate and film, respectively;  $t$  is film thickness;  $D$  is the indentation diagonal, and  $B_s$  is a coefficient that can be deduced from substrate hardness measurements.

To evaluate  $H_{s0}$  and  $B_s$  values, the hardness of the SiO<sub>2</sub> substrate was measured. The relation between the measured substrate hardness,  $H_s$ , and the reciprocal length of the indentation imprints is expressed by the following equation (22)

$$H_s = H_{s0} + B_s/D \quad (2)$$

The values obtained for the SiO<sub>2</sub> substrate,  $H_{s0}$  and the  $B_s$  coefficient, are equal to  $4.3 \pm 0.2$  GPa and  $(29.4 \pm 1.9) \times 10^{-6}$  GPa m, respectively.

To calculate the intrinsic hardness of films, we paid special attention to choose the indentation depths correctly,  $d = D/7$  (for Vickers pyramidal indenter), i.e., in the range where the applied model is valid. The  $d/t = D/7t$  range for the deposited rhodium and iridium boride films on SiO<sub>2</sub> substrates was 0.5–19.3, perfectly lying in the substrate-dominated mixed region, where the film is fractured conforming to the plastically deforming substrate (23). In this  $d/t$  range, the results obtained using the Jönsson and Hogmark model have been demonstrated to coincide quite well with estimations resulting from more complicated models (23, 24).

For the film hardness measurements, indentations were made applying 8 loads, ranging from 0.147 N up to 9.806 N. For each sample, approximately 10–15 random indentations were made at each load.

### 3. RESULTS AND DISCUSSION

Initially, PLD deposition of films was carried out varying the substrate temperature parameter. The following temperatures were investigated: room temperature, 300, and 600 °C. According to our experimental data, depositing at

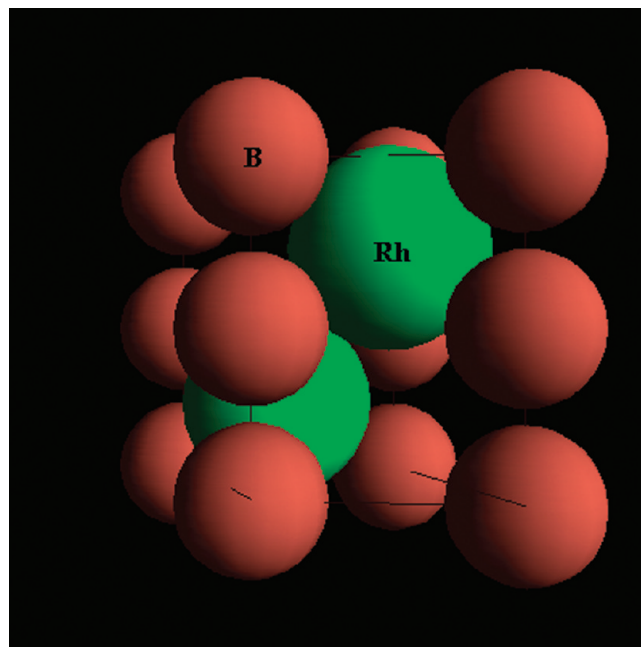


FIGURE 2. RhB<sub>1.1</sub> hexagonal crystal structure.

room temperature, the films were not crystalline, characterized by an irregular surface morphology. As to the deposition at 300 °C, also these results were not satisfying, because the film's surface was very irregular. Therefore, further investigation was performed only for the films deposited at 600 °C.

The X-ray diffractogram of the deposited Rh boride film is reported in Figure 1. Phase analysis demonstrates that the film has the same composition of the target, i.e., it is composed of RhB<sub>1.1</sub>, possessing hexagonal crystal structure (Figure 2, space group  $P6_3/mmc$ , No. 194,  $a = 3.309$  Å,  $c = 4.224$  Å (25), card number 73–1845). The refined structural parameters obtained for the film are  $a = 3.3048$  Å,  $c = 4.2283$  Å, with an isotropic rms microstrain value of 0.00228 and a crystallite size estimated to be in the submicrometer range.

The diffractogram of iridium boride film is reported in Figure 3. Phase analysis of the pattern demonstrates that the film possesses a different composition from that of the target (IrB<sub>1.35</sub>), being composed of IrB<sub>1.1</sub>. The pattern also shows some weak unidentified peaks, indicated with asterisks, that are probably due to surface crystallization of the fused silica glass substrate during contact with hot ablation products.

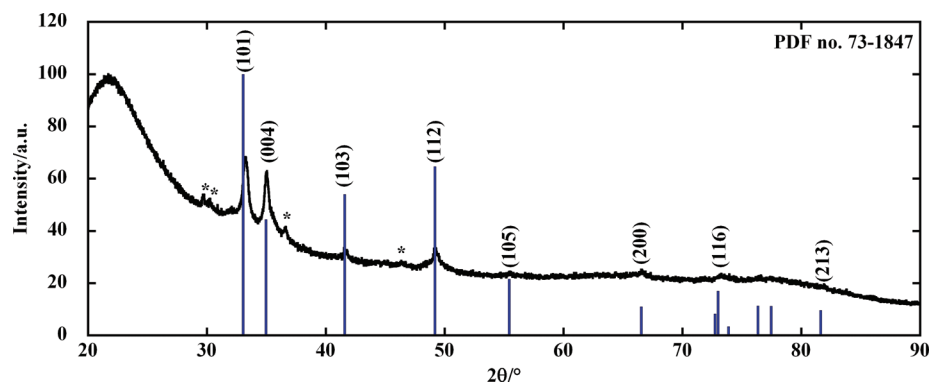


FIGURE 3. X-ray powder diffraction pattern of IrB<sub>1.1</sub> film.

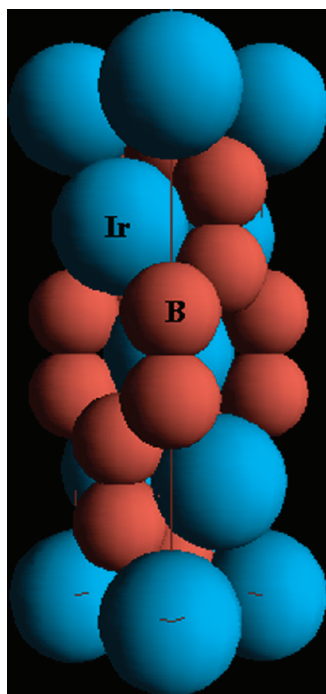


FIGURE 4. IrB<sub>1.1</sub> tetragonal crystal structure.

Unlike IrB<sub>1.35</sub>, which is monoclinic (25) (card number 17–0371), IrB<sub>1.1</sub> possesses tetragonal crystal structure (Figure 4, space group *I4<sub>1</sub>/amd*, No. 141,  $a = b = 2.81 \text{ \AA}$ ,  $c = 10.263 \text{ \AA}$  (25), card 73–1847). Literature data on the binary Ir–B system confirm the existence of IrB<sub>1.35</sub> and IrB<sub>1.1</sub> compounds (26). The refined structural parameters obtained for the deposited film are  $a = b = 2.819 \text{ \AA}$ ,  $c = 10.321 \text{ \AA}$ , with the isotropic rms microstrain value of 0.00093. The IrB<sub>1.1</sub> film presents a slight preferred orientation along the [004] direction. This effect was taken into account during the refinement procedure applying a March–Dollase model (27, 28). By using this model, we obtained a March–Dollase coefficient value of 0.977. The crystallite size was estimated to be in the tens of nanometers range.

From the SEM observations (Figures 5 and 6), it could be concluded that both the film samples exhibit very similar morphology, the films surface being continuous and uniform and having a compact and dense globular grain texture. In Figures 5 and 6, the plain view images are shown at 5 000x magnification. It should be noted that the morphology and the aspect of RhB<sub>1.1</sub> and IrB<sub>1.1</sub> films is very similar to that of

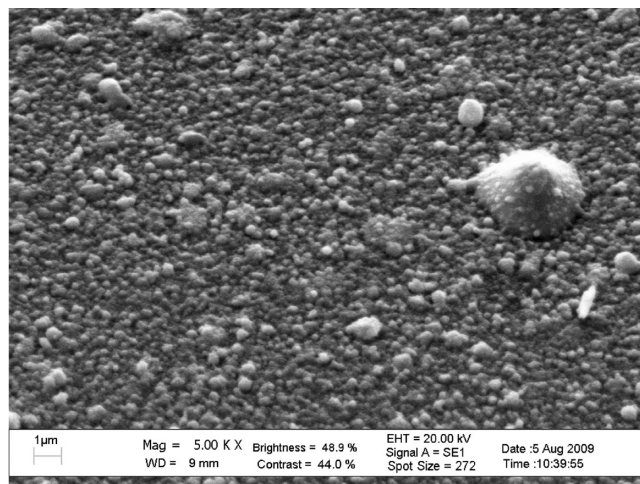


FIGURE 5. SEM micrographs of RhB<sub>1.1</sub> film on SiO<sub>2</sub> substrate at 5000× magnification.

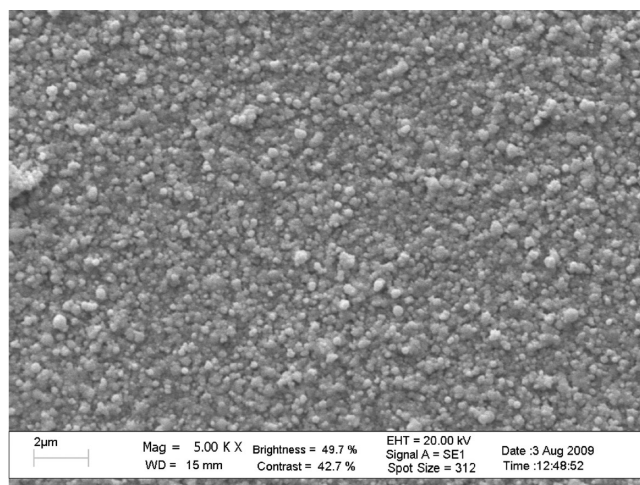


FIGURE 6. SEM micrographs of IrB<sub>1.1</sub> film on SiO<sub>2</sub> substrate at 5000× magnification.

the ReB<sub>2</sub> and RuB<sub>2</sub>–Ru<sub>2</sub>B<sub>3</sub> films reported by us previously (11, 12). All the mentioned films were deposited by PLD using a femtosecond laser source.

The film thickness was obtained from the cross-section SEM images. The Rh boride film on SiO<sub>2</sub> substrate was measured to be  $1.0 \pm 0.2 \mu\text{m}$  thick, whereas that of the Ir boride film on the same substrate was  $0.4 \pm 0.1 \mu\text{m}$  thick. The films thickness values measured by SEM were con-

**Table 1. Vickers Hardness of Some Transition Metal Boride Films**

	thickness ( $\mu$ )	intrinsic film hardness (GPa)
Biphasic RuB <sub>2</sub> –Ru <sub>2</sub> B <sub>3</sub> film(12)	0.7 $\pm$ 0.1	49 $\pm$ 6
RhB <sub>1.1</sub> film (this work)	1.0 $\pm$ 0.2	44 $\pm$ 6
ReB <sub>2</sub> film(11)	0.3 $\pm$ 0.1	52 $\pm$ 6
IrB <sub>1.1</sub> film (this work)	0.4 $\pm$ 0.1	43 $\pm$ 5

firmed also by AFM. The consistent results of both the measurements are presented in Table 1.

Such a difference in film thickness under equal pulsed laser deposition conditions can be likely explained by different ablation efficiency of the two materials. In fact, the ablation efficiency depends on the thermophysical properties of target material (29). A precise description of the short-pulse laser ablation mechanism (which was out of the scope of the present work) is a difficult task requiring more experimental data; however, a simplified qualitative interpretation of the obtained results can be made. The thickness of the RhB<sub>1.1</sub> film is about 1.0  $\mu$ m (film composed of submicrometer crystallite size), whereas that of the IrB<sub>1.1</sub> film is 0.4  $\mu$ m (film composed of nm crystallite size). Therefore, under the equal deposition conditions, larger particles will form a thicker layer at equal deposition time. Another simple consideration is that the atomic weight of Rh is 103, whereas Ir is much heavier, its atomic weight is 192. It was observed in ref 29 that the expansion velocity (during the short-pulse ablation process) is larger for copper than for gold. The larger velocities of the copper species were attributed to their atomic weight, which is about three times smaller than that of gold. In our case, RhB<sub>1.1</sub> should have a larger expansion velocity, because the atomic weight of Rh is almost two times smaller than that of Ir. Likely, a larger expansion velocity leads to the thicker deposited layer.

The RhB<sub>1.1</sub> film presents a homogeneously textured surface, a wide AFM sampling showing images with an average roughness in the range of 40–50 nm. In Figure 7A, an 8  $\mu$ m  $\times$  8  $\mu$ m image is shown as an example (42 nm roughness), and it is combined to a line profile extracted in correspondence of point 1. The surface appears to be ordered, no preferential orientation of the aggregates being visible. However, to obtain an accurate evaluation of the structures characterizing the surface, a high resolution 2.5  $\mu$ m  $\times$  2.5  $\mu$ m image was collected, corresponding to the square portion evidenced in Figure 7A. This topography (Figure 7B) clearly shows globular structures (as observed also for the IrB<sub>1.1</sub> film), with regular shape and an average surface roughness of 22 nm. From the line profile horizontally extracted in correspondence of point 2, the characteristic dimensions of the spherical aggregates were deduced, ranging from 40 to 180 nm along the *z*-direction, and from 300 to 500 nm along the *x*-direction. These globular aggregates are larger than those observed for the IrB<sub>1.1</sub> film.

The IrB<sub>1.1</sub> film shows a homogeneously textured film surface, which appears to be more ordered than the surface of the RhB<sub>1.1</sub> film, deposited under the same experimental conditions. The random AFM sampling showing images (10

$\mu$ m  $\times$  10  $\mu$ m) with an average roughness of about 30 nm, independently on the explored film portion. In Figure 8A, an example of (10  $\mu$ m  $\times$  10  $\mu$ m) image (600 points/line) is shown, being representative of the overall surface. As can be seen, the texture is characterized by globular-like oriented aggregates. These spherical structures are more resolved in Figure 8B, which is a (2  $\mu$ m  $\times$  2  $\mu$ m) high-resolution zoom of A, evidenced by a square in figure. The calculated average roughness is about 20 nm. In correspondence of point 1, a horizontal line profile was extracted to determine the characteristic dimensions of the globular structures. Indeed, the vertical dimension (*z*) ranges from 20 nm of the smallest aggregates to 140 nm of the highest; the lateral (*x*) dimensions are estimated from 80 nm to 200 nm, being affected by the intrinsically lower lateral resolution of the AFM microscope.

Finally, to examine the mechanical properties of films, we carried out Vickers microindentation measurements. In Figures 9 and 10, the experimental plots of the measured composite film/substrate hardness (*H<sub>c</sub>*) versus the applied load for the RhB<sub>1.1</sub> and IrB<sub>1.1</sub> film samples are shown. The intrinsic film hardness values, summarized in Table 1, were calculated applying the “law-of-mixtures” approach, described in the experimental section. As can be seen, both the deposited films are superhard: 44 GPa hardness obtained for RhB<sub>1.1</sub> film and 43 GPa for IrB<sub>1.1</sub> film. In Table 1, the literature data on hardness and thickness of Ru and Re boride films are also included for comparison.

Comparing first the bulk hardness of Re and Ir (both belonging to the sixth period of the periodic table of the elements) borides, it can be observed from Table 2 that bulk hardness is almost the same for ReB<sub>2</sub> and IrB<sub>1.35</sub>, the boron-richest phases in the Re–B and Ir–B systems. However, for the corresponding ReB<sub>2</sub> and IrB<sub>1.1</sub> films, having very close thickness, the intrinsic hardness of the ReB<sub>2</sub> film (52 GPa) is higher than that of the IrB<sub>1.1</sub> film (43 GPa). Likely, the hardness decrease in the latter case could be explained by the decrease in boron content due to the laser ablation process. It is known from the literature (7) that hardness increases with the increase in boron content. This is confirmed also by the authors (31), which observed that the decrease in hardness can be attributed to the boron-deficient structure of ReB<sub>2</sub> single crystals, because a reduction in the number of boron atoms in the crystal would reduce the extent of covalent bonding between the rhenium and boron atoms (the reason for the higher hardness of ReB<sub>2</sub> relative to other materials), and therefore, lower the measured hardness value (31).

The same comparison between the Ru and Rh (both belonging to the fifth period of the periodic table) boride films, biphasic RuB<sub>2</sub>–Ru<sub>2</sub>B<sub>3</sub> and RhB<sub>1.1</sub>, respectively, is not completely correct because of the biphasic nature of Ru borides film. However, one can notice that, at close thickness (within the experimental error), the hardness of Ru borides film is somewhat higher (49 GPa) than that of Rh boride (44 GPa), although the experimental error of 6 GPa makes these difference not significant.

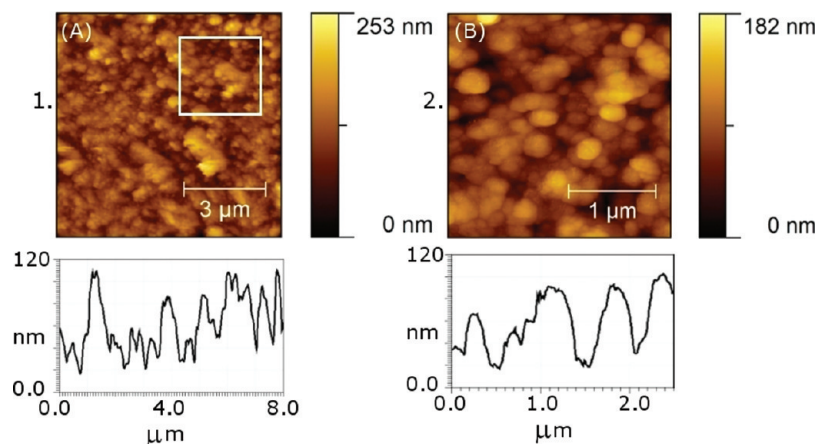


FIGURE 7. AFM images of  $\text{RhB}_{1.1}$  film: (A)  $8 \mu\text{m} \times 8 \mu\text{m}$  image; (B)  $2.5 \mu\text{m} \times 2.5 \mu\text{m}$  zoom of A. Both images are combined with representative line profiles of the surface texture.

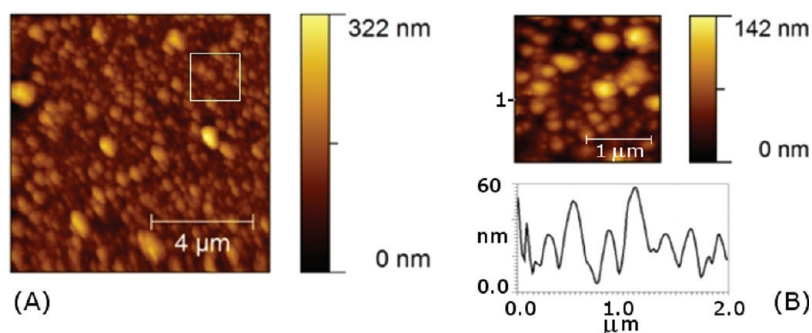


FIGURE 8. AFM images of the  $\text{IrB}_{1.1}$  film: (A)  $10 \mu\text{m} \times 10 \mu\text{m}$  image; (B)  $2 \mu\text{m} \times 2 \mu\text{m}$  zoom of A, plotted with a line profile extracted in correspondence to point 1.

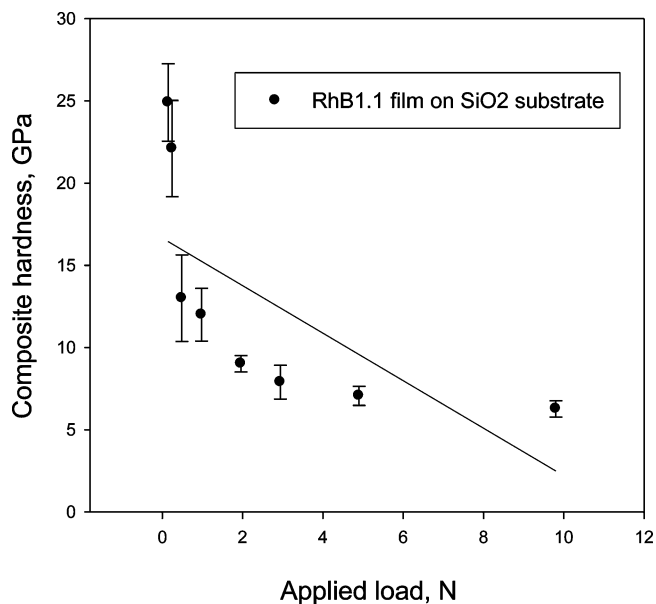


FIGURE 9. Hardness of  $\text{RhB}_{1.1}$  film on  $\text{SiO}_2$  substrate versus applied load.

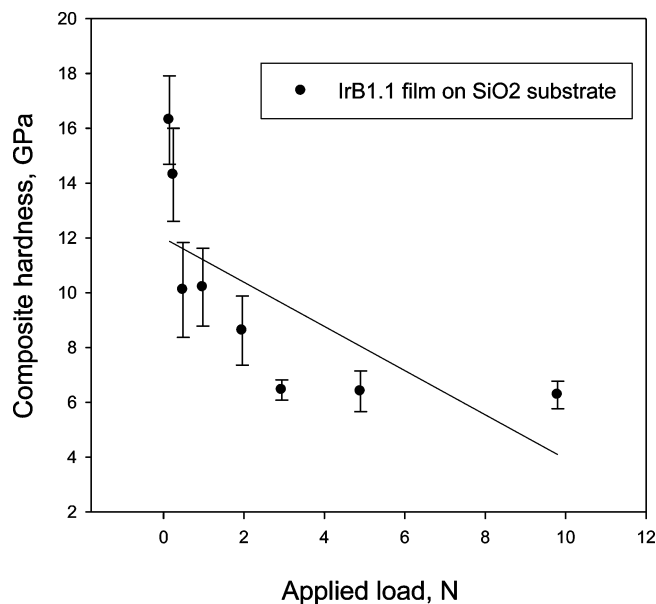


FIGURE 10. Hardness of  $\text{IrB}_{1.1}$  film on  $\text{SiO}_2$  substrate versus applied load.

It should be mentioned that  $\text{RhB}_2$  and  $\text{IrB}_2$  phases are not known. The boron-rich phases in the Rh–B and Ir–B systems are  $\text{RhB}_{1.1}$  and  $\text{IrB}_{1.55}$ , respectively (30).

Regarding the bulk hardness data, it should be noted that our experimental data on  $\text{RuB}_2$  hardness, published in ref 12 and the data obtained by authors (10) are in good agreement. For example, at 0.49 N of applied load our

measured Vickers hardness is 17 GPa (12) and 20.6 GPa the hardness published in ref 10; at 1 N, the values are 14.8 (12) and 16.7 GPa (10), and at 2 N the values are very close, 14.3 (12) and 14.4 GPa (10).

The same good agreement can be noted for the  $\text{ReB}_2$  bulk hardness data. At 0.49 N, our measured Vickers hardness is 49.9 (11) and 48 GPa the hardness presented

**Table 2. Vickers Bulk Hardness of Some Transition Metal Borides**

applied load (N)	Vickers hardness (GPa)			
	RuB <sub>2</sub> (12)	RhB <sub>1.1</sub> (8)	ReB <sub>2</sub> (11)	IrB <sub>1.35</sub> (8)
0.49	17.0	22.6	49.9	49.8
0.98	14.8	16.2	35.5	37.9
1.96	14.3	14.1	34.3	29.0
2.94	11.8	10.2		22.2
4.90	11.2	7.3	25.6	21.3
9.81	10.9	7.0	20.8	18.2

in ref 5, whereas at 5 N, the values are 25.6 (11) and 30.1 GPa (5), correspondingly.

#### 4. CONCLUSIONS

The first successful deposition of rhodium and iridium boride films on SiO<sub>2</sub> substrates (kept at 600 °C) has been performed, applying pulsed laser deposition technique (femtosecond laser source). For film deposition, the RhB<sub>1.1</sub> and IrB<sub>1.35</sub> targets were used. In the case of the RhB<sub>1.1</sub> target, the corresponding film preserved the composition of the target, whereas in the case of IrB<sub>1.35</sub>, the film composition was characterized by a lower boron content, namely IrB<sub>1.1</sub>.

The refined structural parameters obtained for the RhB<sub>1.1</sub> film are  $a = 3.3048$  Å,  $c = 4.2283$  Å, with an isotropic rms microstrain value of 0.00228 and a crystallite size estimated to be in the submicrometer range. The refined structural parameters obtained for the IrB<sub>1.1</sub> film are  $a = b = 2.819$  Å,  $c = 10.321$  Å, with an isotropic rms microstrain value of 0.00093. The IrB<sub>1.1</sub> film presents a slight preferred orientation along the [004] direction, characterized by the March–Dollase coefficient of 0.977. The estimated crystallite size for this film is in the tens of nanometers range.

Both the films exhibit very similar morphology, the film surface being continuous and uniform, characterized by compact and dense globular aggregates texture. The RhB<sub>1.1</sub> film presents a homogeneously textured surface with an average roughness of 20–50 nm, the characteristic dimensions of the globular aggregates being in the range of 40–180 nm along the vertical  $z$ -direction, and of 300–500 nm along the lateral  $x$ -direction. The surface of the IrB<sub>1.1</sub> film possesses a finer texture, slightly more ordered than the surface of the RhB<sub>1.1</sub> film deposited under the same experimental conditions, with an average roughness of 20–30 nm. The characteristic dimensions of the globular structures are in the range of 20–140 nm along the vertical  $z$ -direction, and of 80–200 nm along the lateral  $x$ -direction.

The film thickness was measured to be  $1.0 \pm 0.2$  μm for the RhB<sub>1.1</sub> film, and  $0.4 \pm 0.1$  μm for the IrB<sub>1.1</sub> film. Both the deposited films were found to be superhard, with the

intrinsic hardness of the RhB<sub>1.1</sub> film being 44 GPa, and that of the IrB<sub>1.1</sub> film being 43 GPa.

**Acknowledgment.** The authors thank Dr. D. Ferro for executing the SEM analysis and Dr. R. Generosi for the help in the AFM measurements.

#### REFERENCES AND NOTES

- (1) Sung, C. M.; Sung, M. *Mater. Chem. Phys.* **1996**, *43*, 1–18.
- (2) Cumberland, R. W.; Weinberger, M. B.; Gilman, J. J.; Clark, S. M.; Tolbert, S. H.; Kaner, R. B. *J. Am. Chem. Soc.* **2005**, *127*, 7264–7265.
- (3) Hebbache, M.; Stuparevic, L.; Zivkovic, D. *Solid State Commun.* **2006**, *139*, 227–231.
- (4) Gilman, J. J.; Cumberland, R. W.; Kaner, R. B. *Int. J. Refract. Met. Hard Mater.* **2006**, *24*, 1–5.
- (5) Chung, H. Y.; Weinberger, M. B.; Levine, J. B.; Kavner, A.; Yang, J. M.; Tolbert, S. H.; Kaner, R. B. *Science* **2007**, *316*, 436–439.
- (6) Chung, H. Y.; Weinberger, M. B.; Yang, J. M.; Tolbert, S. H.; Kaner, R. B. *Appl. Phys. Lett.* **2008**, *92*, 261904/1–261904/3.
- (7) Gu, Q.; Krauss, G.; Steurer, W. *Adv. Mater.* **2008**, *20*, 3620–3626.
- (8) Rau, J. V.; Latini, A. *Chem. Mater.* **2009**, *21*, 1407–1409.
- (9) Kaner, R. B.; Gilman, J. J.; Tolbert, S. H. *Science* **2005**, *308*, 1268–1269.
- (10) Weinberger, M. B.; Levine, J. B.; Chung, H. Y.; Cumberland, R. W.; Rasool, H. I.; Yang, J. M.; Kaner, R. B.; Tolbert, S. H. *Chem. Mater.* **2009**, *21*, 1915–1921.
- (11) Latini, A.; Rau, J. V.; Ferro, D.; Teghil, R.; Rossi Albertini, V.; Barinov, S. M. *Chem. Mater.* **2008**, *20*, 4507–4511.
- (12) Rau, J. V.; Latini, A.; Generosi, A.; Rossi Albertini, V.; Ferro, D.; Teghil, R.; Barinov, S. M. *Acta Mater.* **2009**, *57*, 673–681.
- (13) Ivanov, B. L.; Wellons, M. S.; Lukehart, C. M. *J. Am. Chem. Soc.* **2009**, *131*, 11744–11750.
- (14) Latini, A.; Gozzi, D.; Di Pascasio, F. J. *Alloys Compd.* **2002**, *346*, 311–316.
- (15) *Pulsed Laser Deposition of Thin Films*; Chrisey, D. B., Hubler, G. K., Eds.; Wiley: New York, 1994.
- (16) Lutterotti, L.; Matthies, S.; Wenk, H. R. In *Proceedings of the 12th International Conference on Textures of Materials*; Montreal, Aug 9–13, 1999; Materials Research Society: Warrendale, PA, 1999; Vol. 2, pp 15991604.
- (17) Cricenti, A.; Generosi, R. *Rev. Sci. Instrum.* **1995**, *66*, 2843–2847.
- (18) Ferro, D.; Scandurra, R.; Latini, A.; Rau, J. V.; Barinov, S. M. *J. Mater. Sci.* **2004**, *39* (1), 529.
- (19) Ferro, D.; Rau, J. V.; Rossi Albertini, V.; Generosi, A.; Teghil, R. *Surf. Coat. Technol.* **2008**, *202* (8), 1455.
- (20) Joensson, B.; Hogmark, S. *Thin Solid Films* **1984**, *114* (3), 257.
- (21) Iost, A.; Bigot, R. *Surf. Coat. Technol.* **1996**, *80* (1–2), 117.
- (22) Froehlich, F.; Grau, P.; Grellman, W. *Phys. Status Solidi A* **1977**, *42* (1), 79.
- (23) Korsunsky, A. M.; McGurk, M. R.; Bull, S. J.; Page, T. F. *Surf. Coat. Technol.* **1998**, *99* (1–2), 171.
- (24) Puchi-Cabrera, E. S. *Surf. Coat. Technol.* **2002**, *160* (2–3), 177.
- (25) *JCPDS Database*; International Centre for Diffraction Data: Newtown Square, PA, 2001.
- (26) Rogl, P.; Nowotny, H.; Benesovsky, F. *Monatsh. Chem.* **1971**, *102* (3), 678.
- (27) Dollase, W. A. *J. Appl. Crystallogr.* **1986**, *19*, 267–272.
- (28) March, A. *Z. Kristallogr.* **1932**, *81*, 285–297.
- (29) Hermann, J.; Noël, S.; Itina, T. E.; Axente, E.; Povarnitsyn, M. E. *Laser Phys.* **2008**, *18* (4), 374.
- (30) Massalski, T. B. *Binary Alloy Phase Diagrams*; American Society for Metals: Metals Park, OH, Vol. 1, pp 359, 378.
- (31) Levine, J. B.; Nguyen, S. L.; Rasool, H. I.; Wright, J. A.; Brown, S. E.; Kaner, R. B. *J. Am. Chem. Soc.* **2008**, *130*, 16953.

AM9008264